NEOPLASIA
www.neoplasia.com

Volume 12 Number 3 March 2010 pp. 254–263 254

Absence of Glutathione Peroxidase 4 Affects Tumor Angiogenesis through Increased 12/15-Lipoxygenase Activity[1]

Manuela Schneider[*,†], Markus Wortmann[*], Pankaj Kumar Mandal[†], Warangkana Arpornchayanon[*,‡], Katharina Jannasch[§], Frauke Alves[§], Sebastian Strieth[‡], Marcus Conrad[†,2] and Heike Beck[*,2]

[*]Walter Brendel Center of Experimental Medicine, Ludwig-Maximilians-University, Munich, Germany; [†]Institute of Clinical Molecular Biology and Tumor Genetics, Helmholtz Zentrum München, German Research Center for Environmental Health, Munich, Germany; [‡]Department of Otorhinolaryngology, Ludwig-Maximilians-University, Munich, Germany; [§]Department of Hematology and Oncology, University Medicine Göttingen, Göttingen, Germany

Abstract

The selenoenzyme glutathione peroxidase 4 (GPx4) has been described to control specific cyclooxygenases (COXs) and lipoxygenases (LOXs) that exert substantiated functions in tumor growth and angiogenesis. Therefore, we hypothesized a putative regulatory role of GPx4 during tumor progression and created transformed murine embryonic fibroblasts with inducible disruption of GPx4. GPx4 inactivation caused rapid cell death *in vitro*, which could be prevented either by lipophilic antioxidants or by 12/15-LOX–specific inhibitors, but not by inhibitors targeting other LOX isoforms or COX. Surprisingly, transformed *GPx4*$^{+/-}$ cells did not die when grown in Matrigel but gave rise to tumor spheroids. Subcutaneous implantation of tumor cells into mice resulted in knockout tumors that were indistinguishable in volume and mass in comparison to wild-type tumors. However, further analysis revealed a strong vascular phenotype. We observed an increase in microvessel density as well as a reduction in the number of large diameter vessels covered by smooth muscle cells. This phenotype could be linked to increased 12/15-LOX activity that was accompanied by an up-regulation of basic fibroblast growth factor and down-regulation of vascular endothelial growth factor A protein expression. Indeed, pharmacological inhibition of 12/15-LOX successfully reversed the tumor phenotype and led to "normalized" vessel morphology. Thus, we conclude that GPx4, through controlling 12/15-LOX activity, is an important regulator of tumor angiogenesis as well as vessel maturation.

Neoplasia (2010) 12, 254–263

Abbreviations: αSMA, α-smooth muscle actin; bFGF, basic fibroblast growth factor; COX, cyclooxygenase; ECM, extracellular matrix; FITC, fluorescein isothiocyanate; fpVCT, flat-panel volume computed tomography; GPx4, glutathione peroxidase 4; HODE, hydroxy octadecadienoic acid; LOX, lipoxygenase; MEF, murine embryonic fibroblast; MTT, thiazolyl blue tetrazolium bromide; PlGF, placenta growth factor; TAM, 4-hydroxy-tamoxifen, tamoxifen; tMEF, transformed murine embryonic fibroblast; VEGF-A, vascular endothelial growth factor A

Address all correspondence to: Dr. Heike Beck, Walter Brendel Center of Experimental Medicine, Ludwig-Maximilians-University, Marchioninistr. 15, 81377 Munich, Germany. E-mail: heike.beck@med.uni-muenchen.de; or Dr. Marcus Conrad, Institute of Clinical Molecular Biology and Tumor Genetics, Helmholtz Zentrum München, German Research Center for Environmental Health, Marchioninistr. 25, 81377 Munich, Germany. E-mail: marcus.conrad@helmholtz-muenchen.de

[1]This work was supported by the DFG-Priority Programme SPP1190 to H.B., M.C., and F.A.

[2]These authors contributed equally to this work.

Received 19 October 2009; Revised 22 December 2009; Accepted 29 December 2009

DOI 10.1593/neo.91782

Introduction

The selenoenzyme glutathione peroxidase 4 (GPx4) was initially described as an important intracellular antioxidant enzyme for the protection of membranes by its unique capacity to reduce phospholipid hydroperoxides [1]. Later, GPx4 has been considered to be involved in eicosanoid synthesis by controlling cyclooxygenase (COX) and lipoxygenase (LOX) activities [2]. Because these enzymes require basal amounts of lipid hydroperoxides for their activation [3,4], the modulation of GPx4 activity should effectively influence COX and LOX activities and thus eicosanoid synthesis. Indeed, aberrant arachidonic acid metabolism has been demonstrated to play a crucial role in carcinogenesis and tumor angiogenesis [5]. Thus, pharmacological targeting of GPx4, which in turn influences arachidonic acid metabolism, can be considered as a promising strategy to interfere with the tumor-host communication. Yet, it has remained obscure if there is specificity of GPx4 toward distinct LOX and COX isoforms and if an unbalanced regulation of distinct enzymes may influence tumor development *in vivo* [6]. Our recent study using inducible inactivation of *GPx4* in cells and mice provided unequivocal evidence that GPx4 effectively prevents oxidative stress–induced cell death by specifically controlling 12/15-LOX [7,8]. The impact of 12/15-LOX (or the corresponding human ortholog 15-LOX-1) on carcinogenesis seems quite complex, and its role in cancer development and progression is controversially discussed [9]. 12/15-LOX shows increased expression in normal tissues and benign lesions, but not in carcinomas of the bladder, breast, colon, lung, or prostate [10–14]. However, other studies suggested that the 12/15-LOX product, 13-*S*-hydroxyoctadecadienoic acid (13-HODE), enhances colon carcinogenesis [15]. Moreover, 13-HODE has been shown to enhance cell proliferation and to potentiate the mitogenic response to epidermal growth factor (EGF) in different cell types such as BALB/c 3T3, Syrian hamster embryo (SHE) cells [16], as well as human pancreatic adenocarcinomas [16,17]. In addition, overexpression of the human ortholog 15-LOX-1 induces extracellular signal–related kinase 1/2 phosphorylation, decreased p21 (cip/WAF1) expression, and increased colon cancer growth [18]. Conversely, Kim et al. [19] described an antiproliferative effect of 15-LOX-1 in colorectal cancer cells associated with p53 phosphorylation. In line with these results, Shureiqi et al. reported that 13-HODE induces apoptosis and cell cycle arrest in colorectal cancer cells [20]. Studies analyzing the biological relevance of 12/15-LOX in the vascular system seem similarly inconsistent, and 12/15-LOX has been described to either promote or inhibit neovascularization. Here, we hypothesize a putative regulatory role of GPx4 during carcinogenesis. We strongly believe that our genetic model of inducible GPx4 disruption is an ideal model to study tumor progression and tumor angiogenesis in the context of modified linoleic acid metabolism because GPx4 ablation specifically leads to changes in 12/15-LOX activity.

Materials and Methods

Cell Line and Reagents

The 4-hydroxy-tamoxifen (TAM)–inducible *GPx4* knockout murine embryonic fibroblasts (MEFs) were used as described by Seiler et al. [7]. All cell culture reagents were purchased from Invitrogen (Karlsruhe, Germany). MEFs were cultured at 37°C under 5% CO_2 and 5% O_2 in Dulbecco's modified Eagle medium supplemented with 10% fetal bovine serum, 2 mM L-glutamine, 100 U/ml penicillin, and 100 μg/ml streptomycin. To maintain the viability of the cells after induction of GPx4 deletion by adding TAM, cells were always maintained in the presence of (±)-6-hydroxy-2,5,7,8-tetramethylchromane-2-carboxylic acid (Trolox; 1 μM, #56510; Sigma-Aldrich, Deisenhofen, Germany), a water-soluble analog of α-tocopherol (see MTT Assay for Cell Viability section). Tumor cells were harvested near confluence by brief trypsination in 0.25% trypsin/EDTA solution, washed several times, and placed in sterile phosphate-buffered saline (PBS) shortly before implantation. The pan-COX-inhibitor indomethacin (I7378), the pan-LOX-inhibitor NDGA (N5023), and the 12/15-LOX–specific inhibitors Baicalein (#465119) and PD146176 (P4620) as well as 4-hydroxy-tamoxifen (H7904) were purchased from Sigma-Aldrich. pBJ3Ω *c-Myc* and pUC EJ6.6 *Ha-ras*^{V12} were a kind gift from Dr. Hartmut Land. Each time before performing an *in vitro* or *in vivo* assay, GPx4-deleted cells were thoroughly washed with PBS to remove Trolox. Furthermore, an aliquot of the cells was checked for GPx4 expression by quantitative polymerase chain reaction (PCR; see below). As a second control, another aliquot was plated under normal cell culture conditions without adding Trolox, and cell death was analyzed within the next 48 to 72 hours (see below).

Transformation of Conditional GPx4-Deficient MEFs

For oncogenic transformation, *GPx4*-deficient MEFs were cotransduced with *c-Myc*– and *ha-ras*^{V12}–expressing lentiviruses. Soft agar assays were conducted to select for transformed cells. The assay was performed in 60-mm dishes (BD Falcon; Becton Dickinson, Heidelberg, Germany) containing two layers of soft agar. The top and bottom layers were 0.3% and 0.4% agarose, respectively, in Dulbecco's modified Eagle medium supplemented with 10% fetal bovine serum. A total of 2×10^4 of the *c-Myc*– and *ha-ras*–infected cells were added to the top layer before pouring. Single-cell colonies were isolated approximately 2 to 3 weeks after culturing at 37°C and 5% CO_2. Single-cell clones were individually expanded, and GPx4 deletion was tested later in each of the established cell lines by adding TAM (±Trolox) followed by analysis of GPx4 expression (see quantitative reverse transcription [RT]–PCR) and cell death, respectively (see MTT Assay for Cell Viability section).

Immunoblot Analysis

Cell lysates and tumor tissue lysates, protein concentration determination, and immunoblot analysis of GPx4 were performed as described previously [7]. *Ha-ras*^{V12} and *c-Myc* expression was confirmed using anti–*Ha-ras* (#3965; Cell Signaling Technology, New England Biolaboratories, Frankfurt am Main, Germany) and anti–*c-Myc* antibodies (sc-788; Santa Cruz Biotechnology, Heidelberg, Germany).

MTT Assay for Cell Viability

Cells were plated in 96-well plates at 1×10^4 cells per well and incubated overnight. Cells were treated either with Trolox (a water-soluble analog of α-tocopherol; #56510; Sigma-Aldrich), with the pan-COX inhibitor indomethacin, the general LOX inhibitor NDGA and the 12/15-LOX-specific inhibitors Baicalein and PD146176 for 72 hours at various concentrations. Then, 10 μl of 5 mg/ml 3-(4,5-dimethylthiazol-2-yl)-2,5-diphenyltetrazolium bromide (MTT; M2003; Sigma-Aldrich) in PBS was added to 100 μl of culture media. Plates were incubated for 4 hours, and the formazan precipitate was redissolved in 200 μl of 0.04N HCl in isopropanol. The absorbance at

540 nm was recorded using a Sunrise microplate absorbance reader (Tecan, Crailsheim, Germany).

Three-dimensional BD Matrigel Assay

Three days before starting the assay, deletion of *GPx4* was induced by adding TAM to the cell culture medium. To ensure survival of the cells, Trolox, which fully complements GPx4 deficiency *in vitro* (see MTT Assay for Cell Viability section), was given as a supplement to the medium.

Two types of frozen Matrigel (Matrigel as well as Growth Factor–reduced Matrigel; #356234 and #35623; Becton Dickinson GmbH) were thawed overnight at 4°C, and 200 μl of each undiluted Matrigel was placed on 24-well plates and incubated for 1 hour at 37°C. Thereafter, tGPx4 knockout as well as control cells were thoroughly washed with PBS to remove Trolox. Cells were counted and 5×10^4 cells each were reconstituted in 20 μl of culture medium ± TAM. Finally, cells were plated on the BD Matrigel layer, coated with 200 μl of undiluted Matrigel, and incubated for an additional hour at 37°C. Normal cell culture medium ± TAM was added on the top layer. In parallel, the same amount of wild-type and knockout cells was plated on uncoated 24-well plates ± TAM, and GPx4 deletion was verified by analyzing cell death within the next 48 to 72 hours.

The average number of spheroids per well was determined after 14 days of growth in both types of Matrigel. Pictures were taken from triplicate experiments.

RNA Isolation, Reverse Transcription, and Quantitative RT-PCR

Cells were kept 72 hours under the conditions described above adding either TAM and Trolox or Trolox alone to the cell culture medium. Total RNA was extracted with the Qiagen RNA isolation kit (RNeasy Mini Kit #74106; Qiagen, Hilden, Germany), and residual genomic DNA was removed by the RNase-Free DNase Set (#79254; Qiagen). RNA was reverse-transcribed into complementary DNA as described before [21]. Real-time PCR was performed with Lightcycler in a reaction volume of 10 μl using SYBR Green I (LC-FastStart DNA Master^{Plus}, #03 515 885 001; Roche, Mannheim, Germany) according to the manufacturer's protocol. Primers were used at a final concentration of 0.5 μM each. An initial denaturation step at 95°C for 10 minutes was followed by 40 cycles of denaturation (95°C, 1 second), annealing (65°C, 10 seconds), and extension (72°C, 20 seconds). Standard curve was prepared using four dilutions of complementary DNA obtained from mouse embryonic fibroblasts. Relative messenger RNA levels were normalized to β-actin messenger RNA levels in the same samples. Primer sequences are as follows: GPx4 A forward (5′-GCA ACC AGT TTG GGA GGC AGG AG-3′), GPx4 B reverse (5′-CCT CCA TGG GAC CAT AGC GCT TC-3′); β-actin forward (5′-CTA CGA GGG CTA TGC TCT CCC-3′) and reverse (5′-CCG GAC TCA TCG TAC TCC TGC-3′).

In Vivo *Tumor Model*

For *in vivo* implantation studies, cells were kept for at least 72 hours under TAM and Trolox, and the knockout was verified as described above. Before injecting the cells, cells were washed thoroughly with PBS to remove TAM and Trolox. After cell counting, 5×10^6 *c-Myc/Ha-ras^{V12}*–transformed *GPx4*-deficient or *GPx4*-proficient MEFs diluted in 100 μl of sterile PBS were implanted subcutaneously into the flanks of C57BL/6 or severe combined immunodeficient (SCID) mice, respectively. Tumors were collected 16 days after implantation (n = 8 mice per group). Tumor volume was calculated by caliber measurement according to the following formula: V (mm^3) = (length × width × high) × π/6. For the *in vivo* pharmacological studies, mice were treated with Baicalein (1.5 mg/kg in Tween 20) orally every second day beginning at day 3 after tumor cell implantation.

Mice were kept under standard conditions with food and water *ad libitum* (ssniff, Soest, Germany). All animal experiments were performed in compliance with the German Animal Welfare Law and have been approved by the institutional committee on animal experimentation and the government of Upper Bavaria.

Hematoxylin-Eosin Histology

Five-micrometer sections of 4% (wt./vol. in PBS) paraformaldehyde-fixed and paraffin-embedded tumor material were stained as described [22].

Immunohistochemistry and Image Analysis

Tumor tissue samples were snap frozen in liquid nitrogen and stored at −80°C. Ten-micrometer frozen sections were prepared using a cryotome (HM 560; Microm, Walldorf, Germany) and mounted on poly-L-lysine–coated glass slides (Menzel, Braunschweig, Germany). Immunostaining was performed using a phospho–histone H3 antibody (1:200; # 9701; Cell Signaling Technology, New England Biolaboratories) for proliferating cells, a CD31 antibody (1:800; BM 4086B; Acris Antibodies, Hiddenhausen, Germany) for endothelial cells, an α-smooth muscle cell antibody (1:200, A2547; Sigma-Aldrich) to mark endothelial coverage by vascular smooth muscle cells/pericytes and the ApopTag Peroxidase *In Situ* Apoptosis Detection Kit (S7100; Serologicals Corporation, Millipore, Schwalbach, Germany) for the detection of apoptotic nuclei according to the manufacturers' recommendations. Immunoperoxidase staining was performed using the Vector ABC Kit and Vector DAB Kit (Vector Laboratories, Linaris, Wertheim-Bettingen, Germany).

Quantification of Proliferation and Apoptosis

The number of proliferating or apoptotic cells, respectively, was determined in a genotype-blinded fashion in 10 random microscopic visual fields at 200-fold magnification and quantified using pixel-based thresholds in a computer-assisted image analysis software (KS400 Imaging System; Carl Zeiss Vision, Hallbergmoos, Germany) defined as positively stained area per total area.

Quantification of Blood Vessel Density

The number of total blood vessels was determined in a genotype-blinded fashion by counting the number of blood vessels in 10 random microscopic visual fields at 200-fold magnification. Blood vessel density, defined as percentage of CD31-positive staining per unit area, was quantified using pixel-based thresholds in a computer-assisted image analysis software (KS400 Imaging System; Carl Zeiss Vision).

Quantification of Pericyte-Covered Tumor Vessels

Tumor sections were double-stained with anti-CD31 antibody for endothelial cells, and anti–α-smooth muscle actin (αSMA) antibodies for smooth muscle cells/pericytes. The number of α-smooth muscle cell–covered vessels was determined in a genotype-blinded fashion in 10 random microscopic visual fields at 200-fold magnification.

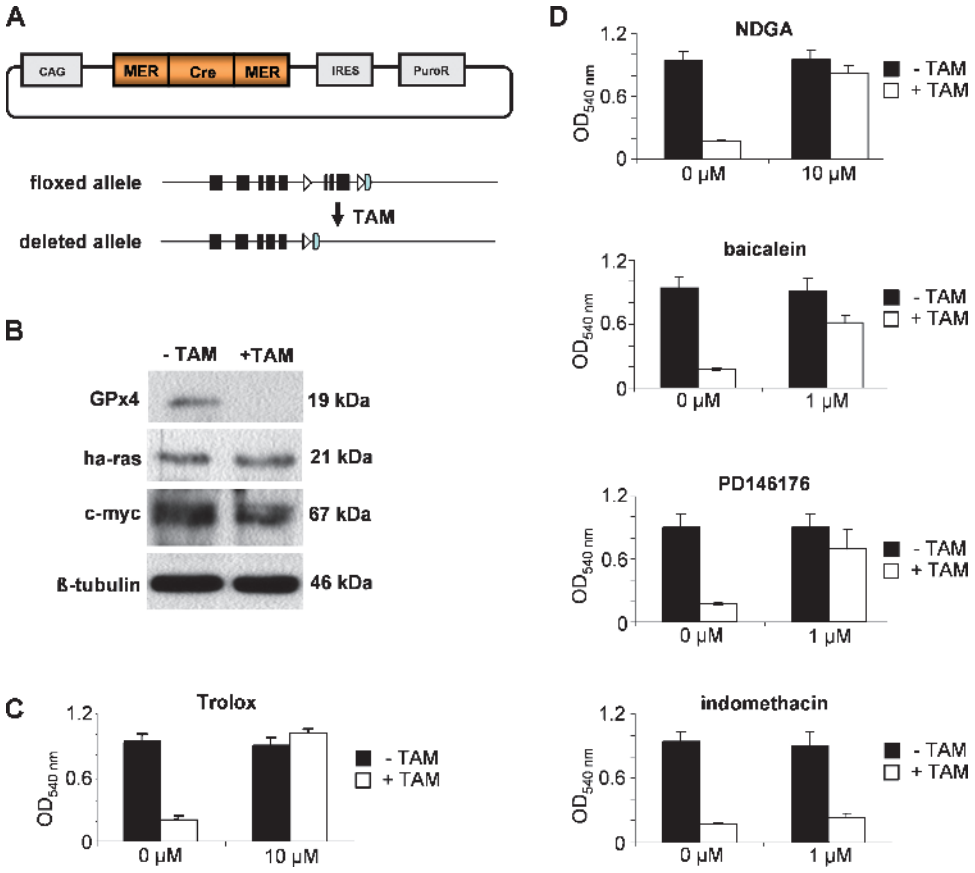

Figure 1. Inducible deletion of GPx4 in transformed cells leads to rapid cell death, which can be prevented by Trolox or 12/15-LOX inhibitors. (A) MEFs isolated from conditional *GPx4* knockout mice were transfected with a TAM-inducible GPx4 knockout system [7]. MERCreMER (*MER* = mutated estrogen receptor) is retained in the cytosol. On addition of TAM, MERCreMER translocates to the nucleus where Cre-mediated deletion of the floxed *GPx4* alleles occurs. (B) Immunoblot analysis with a monoclonal antibody directed against murine GPx4 peptide shows strongly reduced GPx4 protein levels after TAM administration (upper panel). TAM-inducible GPx4 MEFs were transformed with the oncogenes *c-Myc* and *Ha-ras*^{V12} using lentivirus-mediated gene transfer. The expression of both oncogenes was confirmed by immunoblot analysis (lower panel). (C) TAM-induced cell death of *GPx4* knockout MEFs can be prevented by Trolox or (D) by the general LOX inhibitor NDGA and the 12/15-LOX specific inhibitors Baicalein and PD146176 but not by the general COX inhibitor indomethacin. Cell viability was determined 72 hours after TAM treatment by MTT assay. Trolox, NDGA, Baicalein, or PD146176 treatment caused a statistically significant increase in cell viability compared with cell viability in nontreated GPx4-deleted cells.

In Vivo Fluorescence Microscopy

Experiments were performed in male C57BL/6 mice (8-10 weeks old, 25-35 g, n = 4 mice per group). A dorsal skinfold chamber was implanted under anesthesia (subcutaneous injection of 75 mg of ketamine hydrochloride/25 mg xylazine per kilogram body weight) as described [23]. Animals were allowed to recover from the chamber implantation surgery for 2 to 3 days before tumor cells were inoculated into the skinfold chamber preparation.

Before measurement of vessel diameter and vessel density at days 7, 10, and 14 after tumor cell implantation, animals were placed in a polycarbonate tube and were injected intravenously with 0.1 ml of a fluorescein isothiocyanate (FITC)–labeled dextran solution (5% in 0.9% NaCl, M_W = 200,000, FD20; Sigma-Aldrich).

The chamber preparation was mounted on an individually designed microscope stage (Axioplan; Zeiss, Jena, Germany), and tumor vascularization was observed by using a 20× objective (LD acroplan; Zeiss). Epi-illumination was achieved with a 100-W mercury lamp with a fluorescence filter for FITC (excitation, 450-490 nm; emission, 515-525 nm). Images of microvessels in five areas of the tumor were acquired by using a CCD camera (AVC D7; Sony, Tokyo, Japan), displayed on a video monitor and recorded on digital tapes by using a video recorder (SVO-9500MD; Sony) for offline analysis.

Flat-Panel Volume Computed Tomography Imaging

Mice were imaged with flat-panel volume computed tomography (fpVCT), a nonclinical volume computed tomography prototype (GE Global Research, Niskayuna, NY) as described [24,25]. In brief, mice were anesthetized with vaporized isoflurane at 0.8% to 1% concentration, centered on the fpVCT gantry axis of rotation, and placed perpendicularly to the z-axis of the system. At distinct time points, iodine-containing contrast agent, 150 µl of Isovist 300 (Bayer-Schering, Berlin, Germany) per mouse, was applied intravenously approximately 30 seconds before scan, and for better demonstration of small blood vessels, the blood pool agent eXia 160 (Binito Biomedical Inc, Ottawa, Canada) was administered intravenously 90 seconds before each scan as described by Jannasch et al. [25]. All data sets were acquired with the same protocol: 500 views per rotation, 4 seconds rotation time, 360 used detector rows, tube voltage of 80 kilovolt (peak), and a current of 100 mA. A modified Feldkamp algorithm was used for image reconstruction resulting in

isotropic high-resolution volume data sets (512 × 512 matrix, with an isotropic voxel size of approximately 100 μm). For tumor segmentation and volume estimation, data sets were analyzed with voxtools 3.0.64 Advantage Workstation 4.2 (GE Healthcare, UK).

Enzyme-Linked Immunosorbent Assay for Vascular Endothelial Growth Factor A, Placenta Growth Factor, and Basic Fibroblast Growth Factor

Lysates from GPx4 knockout and control tumors as well as cell culture supernatants from both types of cells were prepared, and enzyme-linked immunosorbent assays (ELISAs) for vascular endothelial growth factor (VEGF; MMV00), placenta growth factor (PlGF; MP200), and basic fibroblast growth factor (bFGF, DFB50; all purchased from R&D Systems GmbH, Wiesbaden-Nordenstadt, Germany) were performed as described in the accompanying Quantikine ELISA protocols. All ELISA results were read on a Sunrise microplate absorbance reader (Tecan) at an absorbance of 450 nm, with wavelength correction at 550 nm, and calculated according to the manufacturers' recommendations. Total protein concentrations of tumor homogenates and supernatants were measured with the BCA Protein Assay Kit (#23227; Pierce, Fisher Scientific GmbH, Schwerte, Germany).

Statistical Analysis

Statistical analysis was performed using SigmaStat software. The statistical significance of the results was tested by Student's *t* test. $P < .05$ was considered statistically significant. Results were expressed as mean ± SD.

Results

Transformation of Inducible GPx4 Knockout MEFs with the Oncogenes c-Myc and Ha-ras^{V12}

To investigate the impact of GPx4 depletion on tumorigenesis, we took advantage of our recently established TAM-inducible *GPx4* knockout fibroblasts (Figure 1*A*) [7]. These cells were cotransduced with *c-Myc*– or *Ha-ras^{V12}*–expressing lentiviruses. To establish stably transformed cell lines, colony formation assays were performed, which allowed to isolate single-cell colonies after 2 to 3 weeks of growth in soft agar. Single-cell clones were individually expanded, and the expression of both oncogenes *c-Myc* and *Ha-ras^{V12}* was confirmed by immunoblot analysis (Figure 1*B*). All the following experiments were performed using the *c-Myc*– or *Ha-ras^{V12}*–transformed TAM-inducible *GPx4* knockout fibroblasts (tGPx4).

As shown previously, inducible depletion of GPx4 in nontransformed MEFs caused rapid cell death within 48 hours after knockout induction, which could be prevented either by α-tocopherol or by 12/15-LOX–specific inhibitors. Water-soluble antioxidants and 5-LOX– and COX-specific inhibitors were shown to be ineffective in preventing cell death [7]. To address whether transformed *GPx4* knockout cells behave differently with respect to cell proliferation and cell survival, the knockout was induced by TAM in the presence and absence of Trolox, an α-tocopherol analog, and various LOX and COX inhibitors. Cell viability was determined by MTT assay 72 hours after TAM treatment. As illustrated in Figure 1, *C* and *D*, cell death of transformed *GPx4* knockout cells could be prevented by Trolox, NDGA, Baicalein, and the 12/15-LOX–specific inhibitor PD146176, but not by the COX inhibitor indomethacin. Hence, in terms of cell viability *in vitro*, transformed *GPx4*-null cells do not substantially deviate from the nontransformed parental cell lines.

tGPx4-Deficient MEFs Form Tumor Spheroids in Three-dimensional Extracellular Matrix

One characteristic of tumor cells is their ability to form three-dimensional structures in reconstituted extracellular matrix (ECM) such as BD Matrigel, a solubilized basement membrane preparation extracted from the Engelbreth-Holm-Swarm mouse sarcoma [26]. Interaction of tumor cells with the ECM is thought to be a critical event in controlling angiogenesis and tumor growth. To compare the (tumor cell) behavior of *GPx4*-deficient and -proficient transformed MEFs, cells were plated in between two layers of BD Matrigel to obtain a three-dimensional culture assay.

Unexpectedly, *tGPx4*-null cells embedded in three-dimensional BD Matrigel survived and indeed formed tumor cell colonies (Figure 2*B*). Such colonies were similar in appearance and number (17.53 ± 6.51; Figure 2, *B* and *E*) compared with the colonies formed by control cells (17.60 ± 2.67; Figure 2, *A* and *E*). To test whether survival of *GPx4*-deficient MEFs was dependent on the growth factor content of BD

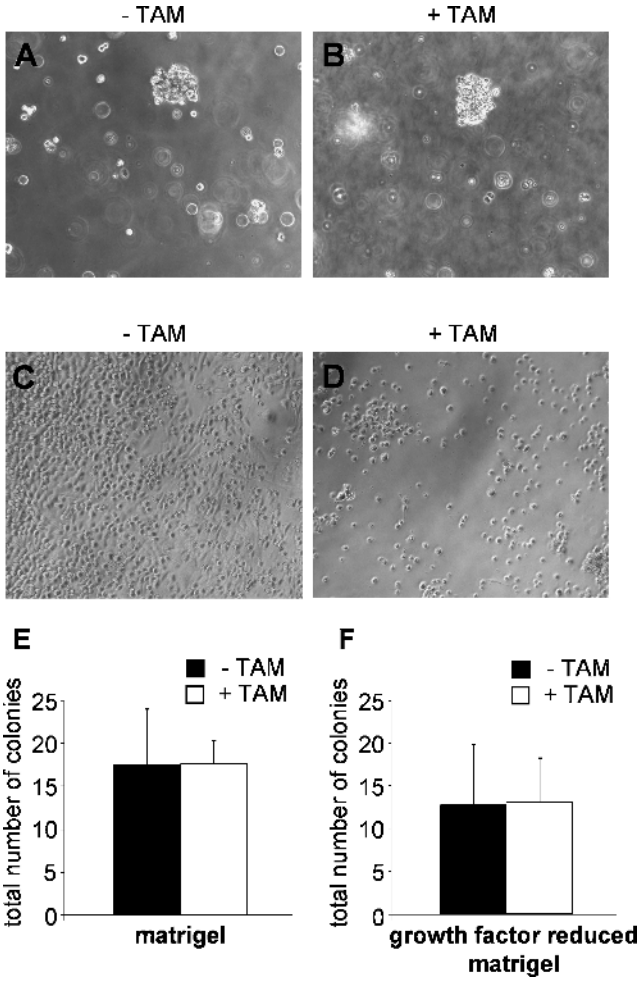

Figure 2. *GPx4* knockout MEFs survive in BD Matrigel. TAM-induced *GPx4* knockout MEFs and uninduced control cells were either embedded in BD Matrigel (A and B) or plated on normal culture dishes (C and D). After 14 days in BD Matrigel, *GPx4* knockout cells formed tumor spheroids (B and E) that were comparable in appearance and number to tumor spheroids formed by control cells (A and E). Similar results were obtained when tumor cells were embedded in Growth Factor–reduced Matrigel (F). In contrast, *GPx4* knockout cells plated on normal dishes died within 48 hours (D).

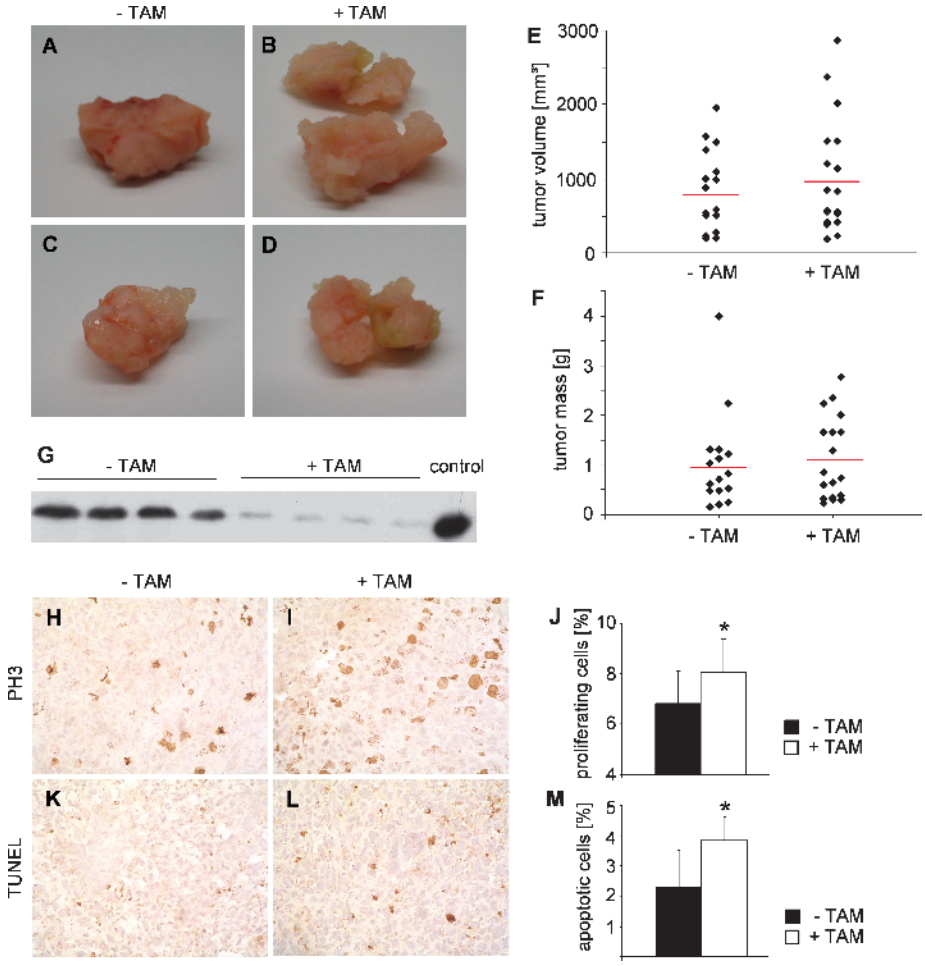

Figure 3. GPx4-deficient transformed MEFs are capable to form tumors *in vivo* (A–D) and display elevated tumor proliferation and apoptosis (H–M). (A–F) *c-Myc*/*Ha-ras*^{V12}–transformed GPx4-deficient MEFs were implanted subcutaneously into C57BL/6 mice. Tumors were collected 16 days after implantation. Control and GPx4 knockout tumors did not show a significant difference in the macroscopic appearance (A–D), tumor volume (E), and tumor mass (F). (G) Deletion of GPx4 in the tumors was confirmed by immunoblot analysis. (H–J) Immunohistologic analysis revealed a higher proliferation rate in *GPx4* knockout tumors (I) compared with control tumors (H) using PH3 antibody as marker for proliferation. (K–M) TUNEL staining demonstrated more apoptotic cells in tumors derived from GPx4-deficient tumor cells (L) compared with control tumors (M).

Matrigel, cell survival and colony formation were tested in parallel in BD Growth Factor–reduced Matrigel. No significant difference in the number of colonies could be found between the two types cells, although the overall number of colonies was reduced under the conditions of limited growth factor availability (12.77 ± 7.07 control colonies *vs* 13 ± 5.24 knockout colonies; Figure 2*F*). In contrast, a strong reduction in cell number of *tGPx4*-null cells seeded on uncoated plates was observed after 48 hours (Figure 2*D*), whereas wild-type cells survived (Figure 2*C*).

Transformed GPx4-Deficient MEFs Form Tumors with Higher Mitotic Activity but Also an Increased Number of Apoptotic Cells

Because transformed *GPx4*-deficient cells died under normal cell culture conditions, but survived and formed colonies when plated in ECM-like BD Matrigel, we asked whether *tGPx4*-deficient cells generate tumors *in vivo*. To this end, *tGPx4*-deficient MEFs and the corresponding noninduced control cells were subcutaneously injected into the flanks of C57BL/6 mice. Tumor growth was monitored every second day, and tumors were harvested and analyzed at day 16 after tumor cell injection. Surprisingly, *GPx4*-deficient and GPx4 control tumors revealed no significant difference with regard to morphologic appearance (Figure 3, *A* and *D*), tumor volume (1399.49 ± 767.21 *vs* 1427.86 ± 1088.49 mm^3; Figure 3*E*) and tumor mass (1.77 ± 0.72 *vs* 1.62 ± 1.58 g; Figure 3*F*). To exclude the possibility that tumors arose from noninduced wild-type cells in the TAM-treated group, GPx4 expression in tumor tissue was analyzed by immunoblot analysis with a GPx4-specific antibody. As illustrated in Figure 3*G*, tumor lysates showed strongly reduced GPx4 expression, indicating that tumors were indeed derived from *tGPx4*-null cells.

Interestingly, immunohistochemical staining using the proliferation marker phospho–histone H3 revealed an increase in the proliferation rate of *GPx4*-deficient tumors (8.08 ± 2.07%) compared with control tumors (6.82 ± 2.08%; Figure 3, *H–J*). Whereas tumors from both groups displayed regions of necrosis, the portion of apoptotic cells was higher in *GPx4*-deficient tumors (3.85 ± 0.78%) than in control tumors (2.30 ± 1.22%) as detected by TUNEL staining (Figure 3, *K–M*).

To quantitate the precise tumor growth and progression over time in a noninvasive fashion, we applied the high-resolution imaging technique, fpVCT. By virtual isolation of the tumor from the acquired isotropic high-resolution fpVCT data sets, tumor volumes were calculated automatically by considering all three dimensions, allowing the generation of precise growth kinetics for each tumor over time. Single fpVCT scans of the entire mice after application of an iodine-containing contrast agent were performed three times per week beginning at day 3 after tumor cell inoculation. In addition, at day 7 and day 14 after tumor cell implantation, we applied the blood pool contrast agent eXia 160 to illustrate the intratumoral vascular network as well as the vessel recruitment from the host in response to the developing tumor. Evaluation of *GPx4*-deficient tumors and control tumors over time by fpVCT imaging yielded no differences in tumor size and progression. Furthermore, contrast medium–containing blood vessels with sizes greater than 150 μm in diameter around and within the tumors were determined. The observed recruitment of host vessels by the tumors as well as the characteristics of large diameter tumor vessels was comparable within the two groups (Figure 4, *A–D*).

Increased Number of Microvessels in GPx4-Deficient Tumors

GPx4-deficient tumors displayed a higher rate of apoptotic cells, nevertheless an increase in tumor cell proliferation. Therefore, no significant alterations about tumor size, tumor weight, or growth rate could be determined between GPx4-deficient tumors and control tumors. In the next step, we performed CD31 immunostaining to evaluate tumor vascularization. Analysis of serial sections for the CD31-positive area demonstrated a markedly increased number of small microvessels in *GPx4*-deficient tumors (total vessel number, 364 ± 119.21), whereas control tumors displayed decreased total vessel numbers (279.73 ± 83.79; Figure 5, *A–D*). However, it is noteworthy that, in control tumors, the mean vessel area was clearly augmented compared with GPx4 knockout tumors (mean ±SEM: 100.26 ± 10.35 *vs* 83.94 ± 12.69 μm^2).

To analyze the density of effectively perfused tumor vessels *in vivo*, *tGPx4*-deficient MEFs and control cells were implanted into the dorsal skinfold chamber. Tumor cells were implanted 3 days after chamber preparation, and *in vivo* fluorescence microscopy was performed at days 7, 10, and 14 after intravenous administration of FITC-dextran, respectively. At days 7 and 10, no differences were observed in vessel diameter and vessel density between *GPx4*-deficient and control tumors. However, at day 14, *GPx4*-null tumors showed a significantly higher functional microcapillary density (262.96 ± 13.72) than control tumors (202.26 ± 13.97; Figure 5, *E–G*), whereas control tumors had a significantly increased tumor vessel diameter and caliber size (15.93 ± 0.60 *vs* 9.95 ± 0.47; Figure 5, *E*, *F*, and *H*).

Decreased Number of αSMA-Covered Vessels

Tumor vessels were also characterized with respect to smooth muscle cell/pericyte coverage by staining tumor sections with anti-CD31 and anti-αSMA antibodies; smooth muscle cell–positive vessels were defined as CD31-positive structures associated with αSMA-positive cells. Analysis of double-stained sections revealed a statistically significant reduction in αSMA-positive vessels in GPx4 knockout tumors when compared with control tumors (7.21 ± 1.81 *vs* 12.25 ± 0.76; Figure 6, *A–C*).

VEGF-A, PlGF, and bFGF Levels of Tumors Derived from tGPx4 Deficient Cells Were Similar to Control Tumors

Because GPx4 knockout tumors displayed a higher microvessel density that was associated with poor mural cell coverage, we wondered if this might be due to an increased endothelial growth factor production by GPx4 knockout tumors. Therefore, we quantified the amount of VEGF-A, PlGF, and bFGF in tumor tissue lysates. Surprisingly, all endothelial growth factor levels obtained from control tumors (VEGF-A, 479.61 ± 220.55 pg/ml; PlGF, 221.41 ± 151.27 ng/μg; bFGF, 272.63 ± 125.33 pg/μg) did not differ from the values obtained from GPx4 knockout tumors (VEGF-A, 555.63 ± 432.29 pg/μg; PlGF, 257.04 ±

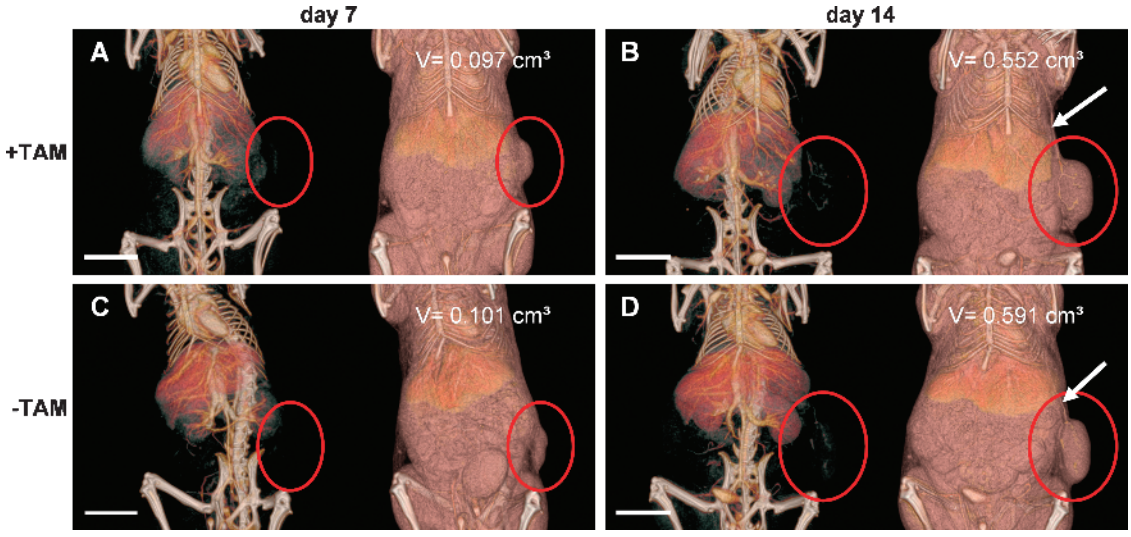

Figure 4. *In vivo* imaging by fpVCT showed no significant alterations for *GPx4*-null tumors. SCID mice with tumors derived from either GPx4-knockout cells or control cells were scanned over time using fpVCT in combination with the blood pool agent eXia 160. Representative pictures from fpVCT data sets show that 7 days after implantation of tumor cells, tumors with comparable volumes formed in both groups (A and C), whereas vessels could not be detected (B and D); red circles indicate tumor localization. Likewise, at the end of the experiment, 14 days after tumor cell implantation, there were no differences in tumor volume and tumor vascularization between the two groups. Note that the tumors of both groups showed similar vessel recruitment (arrows). Scale bars, 10 mm.

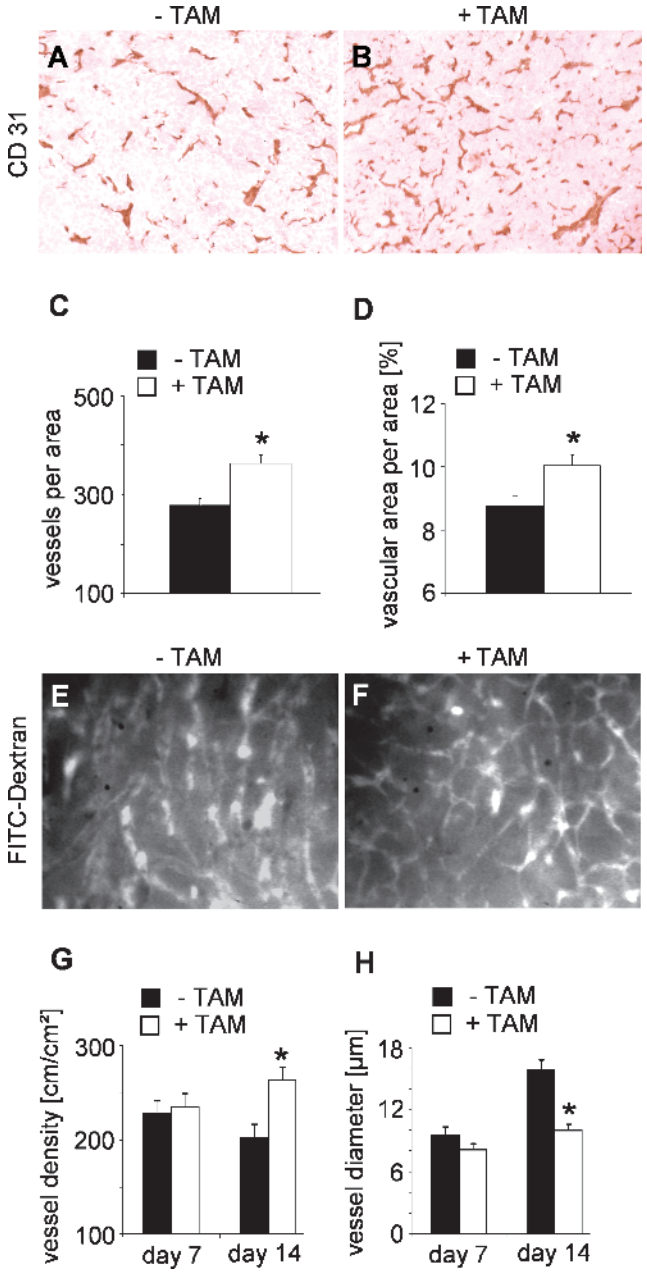

Figure 5. Altered tumor vascularization in *GPx4*-null tumors compared with control tumors. (A–D) Immunohistologic evaluation of CD31-stained tumor sections revealed higher vessel density, in particular more microvessels in *GPx4* knockout tumors. (E–H) For analysis of functional vascular density and vessel diameter, *GPx4*-deficient cells were implanted into the dorsal skinfold chamber preparations in mice. The microvessel density in knockout tumors is significantly increased (E–G). However, newly formed vessels had thinner diameter and markedly reduced vessel lumina in contrast to control tumors (E, F, and H).

83.82 ng/µg; bFGF, 233.03 ± 67.26 pg/µg). Because the SD in tumor tissue samples was high, we also analyzed cell culture supernatants after induction of GPx4 deletion (see below).

Increased bFGF and Decreased VEGF-A Levels in Supernatants of GPx4-Deleted tMEFs

Quantification of VEGF-A, PlGF, and bFGF levels in supernatants of GPx4-deleted tMEFs and control cells revealed a decrease in VEGF-A protein expression levels (729.4 ± 29.38 pg/µg in control supernatants *vs* 204.8 ± 6.13 pg/µg in GPx4 knockout supernatants), no change in the levels of PlGF (2.49 ± 1.29 ng/µg in control *vs* 2.13 ± 0.76 ng/µg in GPx4 knockout supernatants), as well as a strong increase in bFGF expression levels (14.6 ± 6.37 pg/µg in control *vs* 38.4 ± 8.66 pg/µg in GPx4 knockout supernatants). The increase of bFGF is in accordance with data from the literature describing that the 12/15-LOX product 13-HODE is an inducer of bFGF [27].

Baicalein Treatment of Tumor-Bearing Mice Reverses the Vascular Alterations in GPx4-Deficient Tumors

Baicalein, a specific LOX inhibitor, was originally described as an inhibitor of platelet-type 12-LOX, but later also reported to inhibit human 15-LOX [28]. Moreover, Baicalein has already been successfully used for treating neurological disorders in mice [29,30]. Because cell death of *tGPx4* knockout cells could be prevented by Baicalein *in vitro*, we sought to address whether the effects of GPx4 disruption and perturbed 12/15-LOX activity might be reverted by Baicalein administration *in vivo*. For this reason, *GPx4* knockout and GPx4 control tumor-bearing mice were treated daily by intraperitoneal injections of Baicalein. Immunohistologic analyses of Baicalein-treated tumor tissue revealed a clear reduction in microvessel density (untreated GPx4 knockout tumors 8.40 ± 0.45% *vs* treated knockout tumors 6.54 ± 0.85%; Figure 7, *A–C*), which was accompanied by an increase in tumor vessel diameters and mural cell coverage evaluated by αSMA-positive vessels (untreated GPx4 knockout tumors 7.21 ± 1.81 *vs* treated knockout tumors 9.22 ± 2.55; Figure 7*D*). Tumor vessel density and smooth muscle cell/pericyte coverage in Baicalein-treated control tumors revealed no difference compared with the untreated control group (tumor vessel

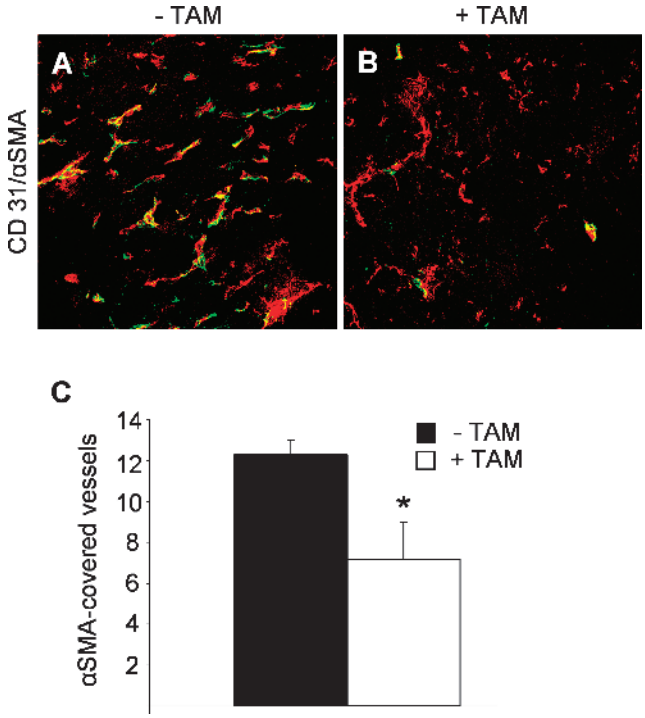

Figure 6. Vessels of *GPx4*-null tumors show diminished pericyte coverage. To further analyze vessel morphology, double staining for CD31 and αSMA was performed on tumor sections (A and B). We observed a reduced number of pericyte covered vessels in GPx4 knockout tumors when compared with control tumors (C).

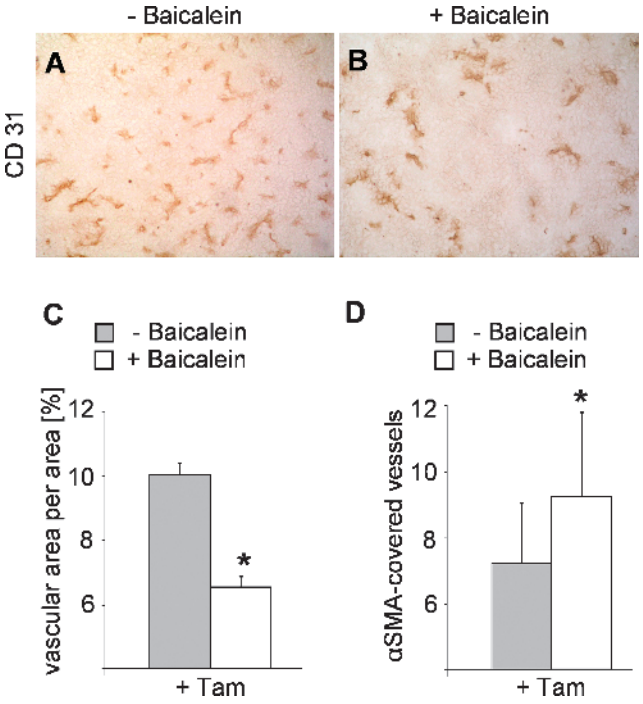

Figure 7. Baicalein treatment reversed the vascular alterations in *GPx4* knockout tumors. The increased microvessel density (A–C) as well as the reduced number of vessels covered by smooth muscle cells in *GPx4* knockout tumors (D) could be reverted by Baicalein administration *in vivo*. Vascular alterations were evaluated by CD31 immunohistochemistry as well as by CD31/αSMA double staining. Note the strong reduction of the overall vascular area (C) as well as the increase of the number of smooth muscle cell covered vessels (D) after Baicalein treatment.

density 8.79 ± 0.29% in untreated control tumors *vs* tumor vessel density 8.40 ± 0.42% in Baicalein-treated control tumors).

Discussion

Numerous studies focusing on the relationship between polyunsaturated fatty acid metabolism and carcinogenesis have identified novel promising compounds targeting COX and LOX activities for anticancer therapies [5,31]. Our recent findings, which identified GPx4 as an important regulator of LOX-catalyzed arachidonic and linoleic acid metabolism by specifically keeping 12/15-LOX activity on a low level [7], prompted us to investigate the function of GPx4 in tumorigenesis and tumor angiogenesis. Therefore, we transformed TAM-inducible *GPx4* knockout MEFs with the oncogenes *c-Myc* and *Ha-ras*^{V12}. Like in the nontransformed parental cell line, inducible GPx4 disruption caused massive cell death *in vitro*, which could be prevented by lipophilic antioxidants such as Trolox as well as by broad-range LOX inhibitors or 12/15-LOX–specific inhibitors.

Contrary to our expectations *tGPx4*-deficient cells survived when embedded into BD Matrigel as well as into Growth Factor–reduced Matrigel and formed three-dimensional "tumor spheroids," which were comparable to spheroids formed by tGPx4 wild-type cells. When implanted subcutaneously into mice, *tGPx4*-deficient cells formed tumors that were indistinguishable from wild-type tumors regarding tumor mass or volume. However, further analysis revealed a strong vascular phenotype.

Tumors derived from tGPx4-deficient cells displayed more microvessels. This phenotype was combined with a reduced number of large diameter vessels as well as a reduction of endothelial tubes covered by smooth muscle cells. Because overexpression of 15-LOX-1 in human prostate cancer cell line PC-3 led to high levels of VEGF-A secretion and therefore enhanced tumor angiogenesis [32], we were interested to analyze whether GPx4-deficient tumors also produce higher levels of VEGF-A. Interestingly, elevated 12/15-LOX activity in tGPx4 cells did not result in increased VEGF-A protein levels in tumor tissues. In addition, neither PlGF nor bFGF protein expression levels were increased *in vivo*. However, analysis of cell supernatants derived from GPx4-deficient and -proficient tMEFs revealed even a decrease of VEGF-A protein expression levels and, at the same time, an increase in bFGF expression levels. The increase of bFGF protein expression levels is in accordance with previous data, showing that the 12/15-LOX product 13-HODE can induce this proangiogenic growth factor. Altogether, results from various studies investigating the biological relevance of 12/15-LOX in the vascular system seem rather inconsistent. 12/15-LOX expression and function have been extensively studied in endothelial cells, smooth muscle cells, and atherosclerotic animal models, where it was shown to play a role in vascular remodeling as well as in the progression of atherosclerotic lesions [33,34]. Conversely, tumor studies demonstrated that the enzyme and its metabolites can either promote or inhibit neovascularization. For example, tumor formation and angiogenesis were inhibited in transgenic mice overexpressing 15-LOX-1 in endothelial cells [35]. In line with these data, Viita et al. [36] showed antiangiogenic action of 15-LOX-1 in a model of hindlimb ischemia. Here, 15-LOX-1 significantly decreased all angiogenic effects induced by VEGF-A and PlGF, including capillary perfusion, vascular permeability, vasodilatation, and increase in capillary number.

One explanation for such inconsistent observations is that 12/15-LOX overexpression might not necessarily result in an increased activity of the enzyme. However, our genetic model of GPx4 ablation leads to increased 12/15-LOX activity, and application of specific 12/15-LOX inhibitors specifically prevents cell death *in vitro*. Interestingly, no up-regulation of 12/15-LOX RNA or protein can be observed after GPx4 deletion. A second explanation might be that various tumor cell types might behave in a different way when exposed to altered 12/15-LOX activity.

By treating our GPx4-deprived tumor-bearing mice with the broad-range LOX inhibitor Baicalein, we could successfully reverse the vascular alterations. Thus, we conclude that GPx4 through controlling 12/15-LOX activity is an important regulator of tumor angiogenesis as well as vessel maturation. Second, modulating 12/15-LOX activity through GPx4 might be an interesting way to reshape tumor vessels.

Acknowledgments

The authors thank Hartmut Land for providing the pBJΩ *c-Myc* and pUC EJ6.6 *Ha-ras*^{V12} plasmids. The authors also thank Wolfgang Schmahl for fruitful discussions, Heidi Förster and Matthias Semisch for excellent technical assistance, and Sarah Greco and Christian Dullin for excellent support running the fpVCT.

References

[1] Ursini F, Maiorino M, Valente M, Ferri L, and Gregolin C (1982). Purification from pig liver of a protein which protects liposomes and biomembranes from peroxidative degradation and exhibits glutathione peroxidase activity on phosphatidylcholine hydroperoxides. *Biochim Biophys Acta* **710**, 197–211.

[2] Imai H, Narashima K, Arai M, Sakamoto H, Chiba N, and Nakagawa Y (1998). Suppression of leukotriene formation in RBL-2H3 cells that overexpressed phospholipid hydroperoxide glutathione peroxidase. *J Biol Chem* **273**, 1990–1997.

[3] Hemler ME, Crawford CG, and Lands WE (1978). Lipoxygenation activity of purified prostaglandin-forming cyclooxygenase. *Biochemistry* **17**, 1772–1779.

[4] Lands WE (1985). Interactions of lipid hydroperoxides with eicosanoid biosynthesis. *J Free Radic Biol Med* **1**, 97–101.

[5] Fürstenberger G, Krieg P, Müller-Decker K, and Habenicht AJR (2006). What are cyclooxygenases and lipoxygenases doing in the driver's seat of carcinogenesis? *Int J Cancer* **119**, 2247–2254.

[6] Conrad M, Schneider M, Seiler A, and Bornkamm GW (2007). Physiological role of phospholipid hydroperoxide glutathione peroxidase in mammals. *Biol Chem* **388**, 1019–1025.

[7] Seiler A, Schneider M, Förster H, Roth S, Wirth EK, Culmsee C, Plesnila N, Kremmer E, Rådmark O, Wurst W, et al. (2008). Glutathione peroxidase 4 senses and translates oxidative stress into 12/15-lipoxygenase dependent– and AIF-mediated cell death. *Cell Metab* **8**, 237–248.

[8] Loscalzo J (2008). Membrane redox state and apoptosis: death by peroxide. *Cell Metab* **8**, 182–183.

[9] Shureiqi I and Lippman SM (2001). Lipoxygenase modulation to reverse carcinogenesis. *Cancer Res* **61**, 6307–6312.

[10] Shureiqi I, Wojno KJ, Poore JA, Reddy RG, Moussalli MJ, Spindler SA, Greenson JK, Normolle D, Hasan AA, Lawrence TS, et al. (1999). Decreased 13-*S*-hydroxyoctadecadienoic acid levels and 15-lipoxygenase-1 expression in human colon cancers. *Carcinogenesis* **20**, 1985–1995.

[11] Shappell SB, Olson SJ, Hannah SE, Manning S, Roberts RL, Masumori N, Jisaka M, Boeglin WE, Vader V, Dave DS, et al. (2003). Elevated expression of 12/15-lipoxygenase and cyclooxygenase-2 in a transgenic mouse model of prostate carcinoma. *Cancer Res* **63**, 2256–2267.

[12] Gonzalez AL, Roberts RL, Massion PP, Olson SJ, Shyr Y, and Shappell SB (2004). 15-Lipoxygenase-2 expression in benign and neoplastic lung: an immunohistochemical study and correlation with tumor grade and proliferation. *Hum Pathol* **35**, 840–849.

[13] Subbarayan V, Xu X, Kim J, Yang P, Hoque A, Sabichi AL, Llansa N, Mendoza G, Logothetis CJ, Newman RA, et al. (2005). Inverse relationship between 15-lipoxygenase-2 and PPAR-gamma gene expression in normal epithelia compared with tumor epithelia. *Neoplasia* **7**, 280–293.

[14] Tang DG, Bhatia B, Tang S, and Schneider-Broussard R (2007). 15-Lipoxygenase 2 (15-LOX2) is a functional tumor suppressor that regulates human prostate epithelial cell differentiation, senescence, and growth (size). *Prostaglandins Other Lipid Mediat* **82**, 135–146.

[15] Hsi LC, Wilson L, Nixon J, and Eling TE (2001). 15-Lipoxygenase-1 metabolites down-regulate peroxisome proliferator–activated receptor gamma via the MAPK signaling pathway. *J Biol Chem* **276**, 34545–34552.

[16] Eling TE and Glasgow WC (1994). Cellular proliferation and lipid metabolism: importance of lipoxygenases in modulating epidermal growth factor–dependent mitogenesis. *Cancer Metastasis Rev* **13**, 397–410.

[17] Yip-Schneider MT, Barnard DS, Billings SD, Cheng L, Heilman DK, Lin A, Marshall SJ, Crowell PL, Marshall MS, and Sweeney CJ (2000). Cyclooxygenase-2 expression in human pancreatic adenocarcinomas. *Carcinogenesis* **21**, 139–146.

[18] Yoshinaga M, Buchanan FG, and DuBois RN (2004). 15-LOX-1 inhibits p21 (Cip/WAF 1) expression by enhancing MEK-ERK 1/2 signaling in colon carcinoma cells. *Prostaglandins Other Lipid Mediat* **73**, 111–122.

[19] Kim J, Baek SJ, Bottone FG, Sali T, and Eling TE (2005). Overexpression of 15-lipoxygenase-1 induces growth arrest through phosphorylation of p53 in human colorectal cancer cells. *Mol Cancer Res* **3**, 511–517.

[20] Shureiqi I, Chen D, Lee JJ, Yang P, Newman RA, Brenner DE, Lotan R, Fischer SM, and Lippman SM (2000). 15-LOX-1: a novel molecular target of nonsteroidal anti-inflammatory drug-induced apoptosis in colorectal cancer cells. *J Natl Cancer Inst* **92**, 1136–1142.

[21] Beck H, Semisch M, Culmsee C, Plesnila N, and Hatzopoulos AK (2008). Egr-1 regulates expression of the glial scar component phosphacan in astrocytes after experimental stroke. *Am J Pathol* **173**, 77–92.

[22] Conrad M, Jakupoglu C, Moreno SG, Lippl S, Banjac A, Schneider M, Beck H, Hatzopoulos AK, Just U, Sinowatz F, et al. (2004). Essential role for mitochondrial thioredoxin reductase in hematopoiesis, heart development, and heart function. *Mol Cell Biol* **24**, 9414–9423.

[23] Yuan F, Salehi HA, Boucher Y, Vasthare US, Tuma RF, and Jain RK (1994). Vascular permeability and microcirculation of gliomas and mammary carcinomas transplanted in rat and mouse cranial windows. *Cancer Res* **54**, 4564–4568.

[24] Missbach-Guentner J, Dullin C, Kimmina S, Zientkowska M, Domeyer-Missbach M, Malz C, Grabbe E, Stühmer W, and Alves F (2008). Morphologic changes of mammary carcinomas in mice over time as monitored by flat-panel detector volume computed tomography. *Neoplasia* **10**, 663–673.

[25] Jannasch K, Dullin C, Heinlein C, Krepulat F, Wegwitz F, Deppert W, and Alves F (2009). Detection of different tumor growth kinetics in single transgenic mice with oncogene-induced mammary carcinomas by flat-panel volume computed tomography. *Int J Cancer* **125**, 62–70.

[26] Kleinman HK and Martin GR (2005). Matrigel: basement membrane matrix with biological activity. *Semin Cancer Biol* **15**, 378–386.

[27] Sen M, McHugh K, Hutzley J, Philips BJ, Dhir R, Parwani AV, and Kelavkar UP (2006). Orthotopic expression of human 15-lipoxygenase (LO)-1 in the dorsolateral prostate of normal wild-type C57BL/6 mouse causes PIN-like lesions. *Prostaglandins Other Lipid Mediat* **81**, 1–13.

[28] Deschamps JD, Kenyon VA, and Holman TR (2006). Baicalein is a potent *in vitro* inhibitor against both reticulocyte 15-human and platelet 12-human lipoxygenases. *Bioorg Med Chem* **14**, 4295–4301.

[29] van Leyen K, Kim HY, Lee S, Jin G, Arai K, and Lo EH (2006). Baicalein and 12/15-lipoxygenase in the ischemic brain. *Stroke* **37**, 3014–3018.

[30] Lapchak PA, Maher P, Schubert D, and Zivin JA (2007). Baicalein, an antioxidant 12/15-lipoxygenase inhibitor improves clinical rating scores following multiple infarct embolic strokes. *Neuroscience* **150**, 585–591.

[31] Pidgeon GP, Lysaght J, Krishnamoorthy S, Reynolds JV, O'Byrne K, Nie D, and Honn KV (2007). Lipoxygenase metabolism: roles in tumor progression and survival. *Cancer Metastasis Rev* **26**, 503–524.

[32] Kelavkar UP, Nixon JB, Cohen C, Dillehay D, Eling TE, and Badr KF (2001). Overexpression of 15-lipoxygenase-1 in PC-3 human prostate cancer cells increases tumorigenesis. *Carcinogenesis* **22**, 1765–1773.

[33] Cyrus T, Witztum JL, Rader DJ, Tangirala R, Fazio S, Linton MF, and Funk CD (1999). Disruption of the 12/15-lipoxygenase gene diminishes atherosclerosis in apo E-deficient mice. *J Clin Invest* **103**, 1597–1604.

[34] Shen J, Herderick E, Cornhill JF, Zsigmond E, Kim HS, Kühn H, Guevara NV, and Chan L (1996). Macrophage-mediated 15-lipoxygenase expression protects against atherosclerosis development. *J Clin Invest* **98**, 2201–2208.

[35] Harats D, Ben-Shushan D, Cohen H, Gonen A, Barshack I, Goldberg I, Greenberger S, Hodish I, Harari A, Varda-Bloom N, et al. (2005). Inhibition of carcinogenesis in transgenic mouse models over-expressing 15-lipoxygenase in the vascular wall under the control of murine preproendothelin-1 promoter. *Cancer Lett* **229**, 127–134.

[36] Viita H, Markkanen J, Eriksson E, Nurminen M, Kinnunen K, Babu M, Heikura T, Turpeinen S, Laidinen S, Takalo T, et al. (2008). 15-Lipoxygenase-1 prevents vascular endothelial growth factor A– and placental growth factor–induced angiogenic effects in rabbit skeletal muscles via reduction in growth factor mRNA levels, NO bioactivity, and down-regulation of VEGF receptor 2 expression. *Circ Res* **102**, 177–184.